Int. J. Adv. Eng. Pure Sci. 2020, 32(2): 185-191
DOI: 10.7240/jeps.627298

RESEARCH ARTICLE / ARAŞTIRMA MAKALESİ

Structure, Microstructure, and Optical Properties of Tb Doped ZnO Nanorods

Tb Katkılı ZnO Nanoçubukların Yapı, Mikroyapı ve Optik Özellikleri

Adil GÜLER[1]

[1]*Marmara University, Ataturk Faculty of Education, Department of Computer and Instructive Technology Teacher, 34722 Goztepe, Istanbul, Turkey*

Abstract
The rare-earth-doped Zinc Oxides (ZnO) are significant materials, especially in photodetector technology, for high detection and high-speed optical communication. Here, important physical properties of Terbium-doped ZnO synthesized by the hydrothermal method were analyzed based on their concentration dependence. Structural behaviors of the nanorods were identified by the X-ray diffraction (XRD) technique and were figured out that $Zn_{1-x}Tb_xO$ samples were hexagonal Wurtzite structure with no secondary phase. The results of the structural behaviors were also proved by Rietveld analysis. The effect of Tb element in $Zn_{1-x}Tb_xO$ composition was clarified by calculating lattice parameters and cell volumes. To define the system better, microstructural parameters were provided by calculation. Scanning Electron Microscope images revealed random agglomeration. Due to the small amount of Tb increment in $Zn_{1-x}Tb_xO$ set, the desired elemental composition results were obtained in the nanorod sets (from x=0 to x=0.05 with the increment x rate of 0.01). By plotting $(F(R_\alpha)\ h\upsilon)^2$ versus hυ, the bandgap energies of $Zn_{1-x}Tb_xO$ structures were determined, and the variation of E_g energies with increasing Tb dopant in the structures were discussed.
Keywords: Zinc oxide, hydrothermal method, diffuse reflectance spectroscopy, nanorods

Öz
Nadir toprak katkılı Çinko Oksitler (ZnO), fotodetektör teknolojisinde özellikle yüksek algılama ve yüksek hızlı optik iletişim için oldukça önemli malzemelerdir. Bu çalışmada, hidrotermal yöntemle sentezlenen Terbium katkılı ZnO'nun önemli fiziksel özellikleri, konsantrasyon bağımlılıklarına göre analiz edilmiştir. Nano çubukların yapısal davranışları, X-ışını kırınımı (XRD) tekniği ile tanımlanmış ve $Zn_{1-x}Tb_xO$ örneklerinin ikincil fazı olmayan altıgen Wurtzite yapı olduğu tespit edilmiştir. Yapısal davranışların sonuçları, Rietveld analiziylede kanıtlanmıştır. Tb elementinin $Zn_{1-x}Tb_xO$ bileşiğindeki etkisi, kafes parametreleri ve hücre hacimleri hesaplanarak saptanmıştır. Yapıyı daha iyi tanımlamak için hesaplama yoluyla mikroyapısal parametreler elde edilmiştir. Taramalı Elektron Mikroskobu görüntüleri rastgele dağılımı ortaya çıkarmıştır. $Zn_{1-x}Tb_xO$ setindeki az miktardaki Tb artışına bağlı olarak, nano çubuk setleri (x = 0' dan x = 0,05'e kadar olan artışlarla) oldukça iyi elementsel kompozisyon sonuçları vermiştir. $(F(R_\alpha)\ h\upsilon)^2$ 'ye karşılık hυ'ye göre, $Zn_{1-x}Tb_xO$ yapılarının bant aralığı enerjileri belirlendi ve yapılardaki artan Tb dopantına bağlı Eg enerjilerinin değişimi tartışıldı.
Anahtar Kelimeler: Çinko oksit, hidrotermal metot, dağıtımlı yansıtma spektroskopisi, nano çubuklar

I. INTRODUCTION

The increasing demands on both energy and technological applications make the materials critical on their physical characteristics with new varying chemical combinations. Zinc oxide (ZnO), a well-known and widely used material with different dopant elements, still keeps the importance on varying miscellaneous properties depending on synthesizing conditions and dopant rates with different elements [1-8]. With the feature of wide band-gap (3.37 eV), semiconductor ZnO occupies a special place at detector technologies with the blue and UV spectral ranges and solid-state light sources [9 and the references therein]. Among the laser material technology, ZnO is one of the conventional material for creating laser diodes and UV light-emitting diodes with the property of 60 meV binding energy, which is higher than the existing binding energy of GaN (25 meV) [9]. The properties of high radiation, thermal and chemical resistance make ZnO a preferable material in the transparent contacts of solar cells. Besides these features, ZnO and its doped forms are used in acoustic, magnetic and electric, optic, cosmetic, and even nuclear applications [10-14].

Corresponding Author: Adil GÜLER, Tel: +90(532)7652866, e-posta: adil.guler@marmara.edu.tr
Submitted: 30.09.2019, **Revised**: 09.02.2020, **Accepted**: 19.02.2020

Moreover, due to fast reset time, high response, photoconductive gain, and more effective area, ZnO-based photodetectors have an important role in commercial applications when compared to the conventional GaN [15-17] or SiC [18] photodetector technologies. In addition, to tailor the intrinsic physical properties such as electronic properties and luminescence, relevant doping elements and their rates in ZnO are essential for application prospects [19]. With the property of its special electron–shell structure, rare earth [RE] ions exhibit a better center by means of luminescence characteristics via their individual 4f electron transition at different energy levels [20 - 22]. It is expected that ZnO nanostructures doped with Tb should be applicable to both micro- and nano-optoelectronics. It is a general information and well known in the literature that the physical and chemical properties of doped-ZnO are heavily affected by the preparation conditions, the dopant rate, and dopant elements such as such as Cr, Co, Fe, V, Mg and Ni [1].

In the present work, the concentration-dependent Tb-doped ZnO samples in nanorod forms were synthesized through hydrothermal method and the structural and optical properties of the samples were analyzed. The results of the outcomes were correlated among the evaluated parameters.

II. MATERIALS AND METHODS

By hydrothermal method, the concentration-dependent Tb-doped ZnO nanorods were synthesized ($Zn_{1-x}Tb_xO$: x=0.00, 0.01, 0.02, 0.03, 0.04, and 0.05) and the used chemicals and preparation method were detailed in Ref. [23]. The possible phases at room temperature were defined by the XRD pattern by using a Rigaku Multiflex XRD instrument with monochromated Cu Kα (1.5418Å) source in the 2θ scan range of 20º to 80º. GSAS Rietveld analysis program was performed to match the obtained pattern and calculated analysis. By the tool of Scanning Electron Microscopy (SEM-EDX) Jeol-6390-LV, the surface morphologies of the samples were evaluated. A Perkin Elmer Spectrum Two FTIR-ATR spectrophotometer was used for defining Tb^{3+} doped ZnO and pure ZnO stretching vibrations. By diffuse reflectance attachments, the optical reflectance properties were defined of the samples by Shimadzu 2600 Plus UV-Spectrophotometer.

III. RESULTS AND DISCUSSIONS

3.1 Structural and morphological analysis

In the range of 20o ≤ 2θ ≤ 80o degrees, XRD patterns of all samples were determined, and the all revealed peak positions in the XRD patterns were indexed without any secondary phase in Fig. 1 (a).

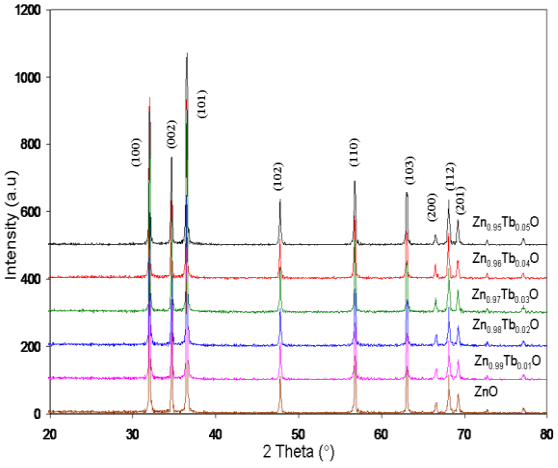

Fig. 1a X-ray diffraction of $Zn_{1-x}Tb_xO$ (from x=0.00 to 0.05 with 0.01 increment) samples.

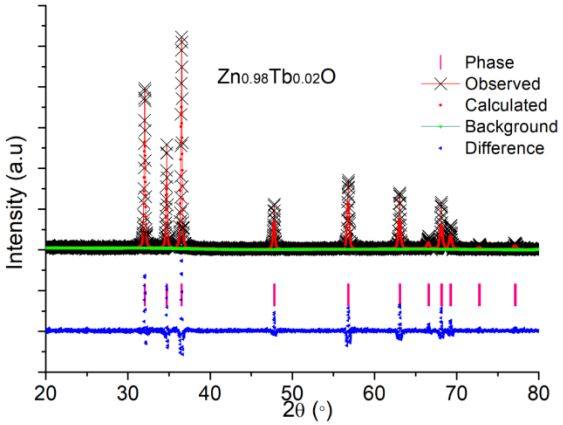

Fig. 1b The Rietveld analysis of $Zn_{0.98}Tb_{0.02}O$ sample.

Rietveld refinement analysis for Zn1-xTbxO concentrations was provided, and for x=0.02 concentration rate, the refinement was plotted as seen in Fig. 1 (b). As seen in Fig. 1 (b) the refinement is highly compatible in terms of a very slight difference between observed and calculated patterns. All phases were matched well with the marked peak positions. We, therefore, conclude that the refinement with the Rietveld method proved the high-quality samples with the crystal structure. The microstructural parameters such as average nanorod sizes, volume of the unit cell, the concentration-dependent, lattice parameters, stress (σ), microstrain (Ɛ), dislocation density (δ) (the amount of defect in the sample), bond length L, and the locality of the atoms and their displacement (u) were determined. The obtained microstructural parameter results from the Rietveld refinement method were reported in Table1 [1].

Table 1. The microstructural variations of formula-dependent $Zn_{1-x}Tb_xO$ nanorods.

	ZnO	**$Zn_{0.99}Tb_{0.01}O$**	**$Zn_{0.98}Tb_{0.02}O$**	**$Zn_{0.97}Tb_{0.03}O$**	**$Zn_{0.96}Tb_{0.04}O$**	**$Zn_{0.95}Tb_{0.05}O$**
a (Å)	3.251	3.245	3.247	3.249	3.243	3.247
c (Å)	5.208	5.2	5.199	5.202	5.2	5.202
c/a	1.601	1.602	1.601	1.601	1.603	1.602
Volume,V($Å^3$)	47.667	47.418	47.473	47.559	47.360	47.499
D (nm)	48.125	49.032	52.297	53.146	54.059	45.442
$\varepsilon*10^{-3}$	0.7202	0.7069	0.6628	0.6522	0.6412	0.7628
$\delta*10^{14}$	0.0004317	0.0004159	0.0003656	0.0003540	0.0003421	0.0004842
U	0.37988	0.37980	0.37998	0.37999	0.37964	0.37984
$\sigma*10^9(N/m^2)$	-23.430	-64.868	-22.930	-22.954	-23.101	-23.418
L (nm)	1.9784	1.9750	1.9757	1.9769	1.9741	1.9761
E_g (eV)	3.199	3.194	3.251	3.209	3.199	3.224

The ε value was observed as the maximum for the dopant ratio of x=0.05 and except for x=0.05 a decrease in ε-values with increment Tb amount was revealed in the structure. The negative signed σ values in Table 1 show compressive stress. In the host lattice structure, the fluctuations in stress and strain values may give rise to much dislocations and physical defects. Therefore, the amount of defects in the sample referring to dislocation density (δ) was also studied. The highest particle size (54.059 nm) was provided for the concentration rate of x=0.04. An increasing tendency was observed in terms of particle sizes with increment of Tb amounts from x=0.00 to x=0.04 and after that concentration, the sizes of particles decreases. Almost no variation was observed in the u parameter (u=0.379) which is almost constant for all $Zn_{1-x}Tb_xO$ concentrations. We therefore conclude that the displacement is almost constant with the increment of Tb in the host lattice structure. Zn-O bond lengths L was calculated around 1.97 which is almost the same for all Tb-doped ZnO nanosystems. Now that the locality of atoms and their displacement was almost constant, this obtained result for L values is in the good harmony with u values.

Figures 2-7 belong to the SEM pictures of pure ZnO and $Zn_{1-x}Tb_xO$ nanorods. Almost perfect cross sections of hexagonal nanorods (consisting of micro-rods) were observed from provided SEM figures. The observed nanorods were divided into two groups depending on rod sizes without any continuous size distributions. The larger and smaller roads showed quite different in terms of sizes from each other as well. When we compared the groups of the specimens in SEM frame, at least 5 times larger in size was observed. Another effect giving rise to vary as size is the increasing Tb amount which is predominant reason in both increasing the number of smaller rods and decreasing the size of smaller rods.

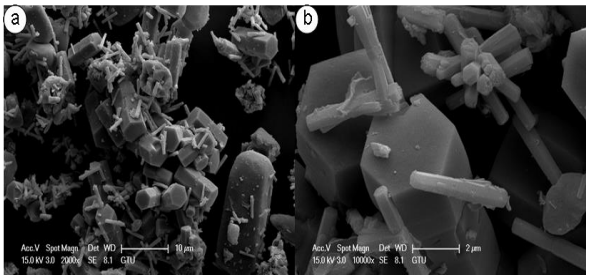

Fig. 2 the micrographical images for ZnO nanorods with varying magnifications.

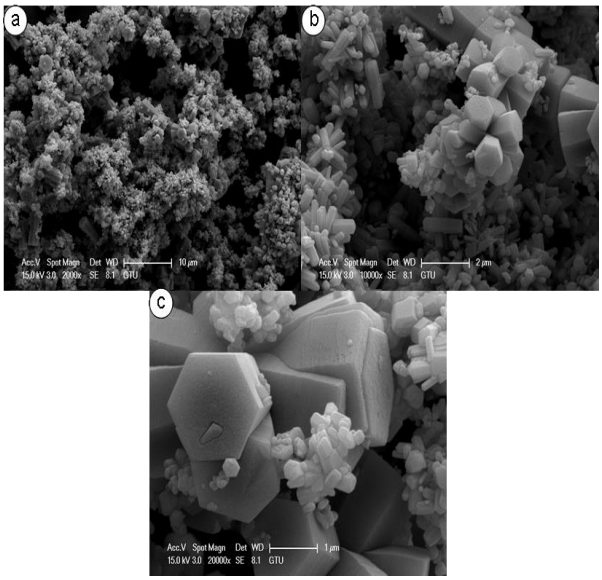

Fig. 3 the micrographical images for $Zn_{0.99}Tb_{0.01}O$ with varying magnifications.

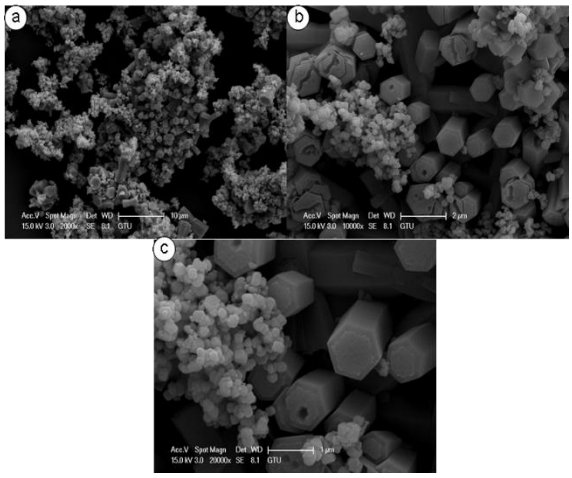

Fig. 4 the micrographical images for $Zn_{0.98}Tb_{0.02}O$ with varying magnifications.

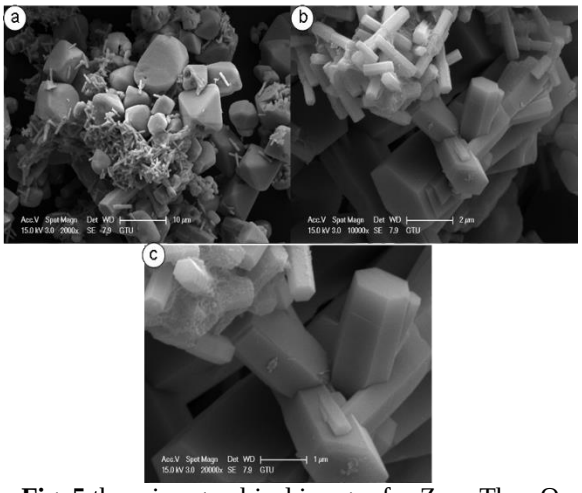

Fig. 5 the micrographical images for $Zn_{0.97}Tb_{0.03}O$ with varying magnifications

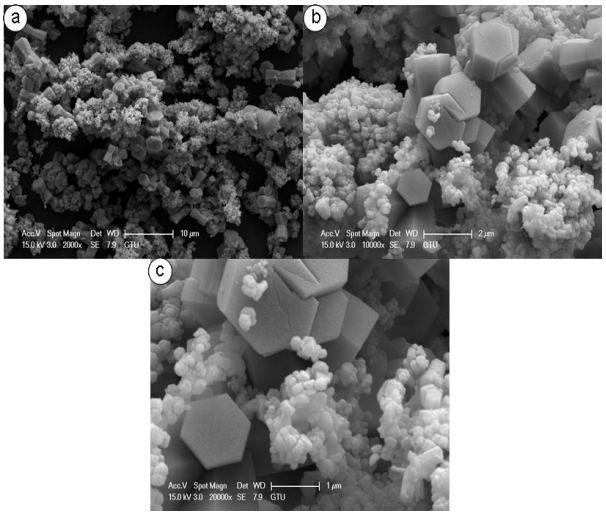

Fig. 6 the micrographical images for $Zn_{0.96}Tb_{0.04}O$ with varying magnifications

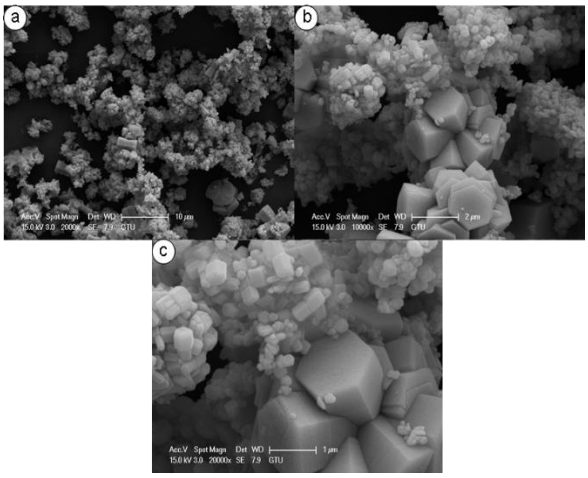

Fig. 7 the micrographical images for $Zn_{0.95}Tb_{0.05}O$ with varying magnifications.

3.2 FTIR analysis

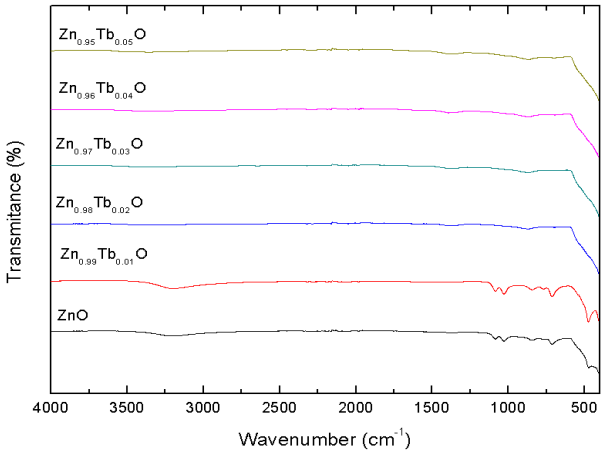

Fig. 8 FTIR spectra of $Zn_{1-x}Tb_xO$ nanorods

Tb^{3+} doped ZnO and the pure ZnO stretching vibrations were depicted in Fig. 8. The observed C-O-C peaks in Fig. 8 are at 1087 and 1025 cm^{-1} belonging to undoped and 1% Tb^{3+}-doped ZnO samples respectively, and no other concentrations (x=0.02, 0.03, 0.04, and 0.05 Tb^{3+} ion-doped ZnO samples) had the same peaks too. Moreover, we conclude that the transformation of $Zn(OH)_2$ to ZnO was completed due to the ZnO peak that reveals between 585 and 475 cm^{-1}. The large band located at 475, 464, and 419 cm^{-1} refers to the ZnO stretching in ZnO lattice in the literature [24- 28]. This stretching after x=0.01 concentration rate was disappeared in our case. In the doped samples, the doping effect of rare-earth ions should play a predominant role in the small shift in the peak positions. The band at 475 cm^{-1} appears for undoped in Fig. 8. This behavior has also been reported for a study on Tb-doped ZnO [29]. These statements were proofed by the FTIR analysis wavenumber results demonstrated in Table 2. In undoped ZnO and $Zn_{0.99}Tb_{0.01}O$ These (O-H, C-O-C, Zn-O) functional groups wave numbers not much have different.

Table 2 FTIR spectra results of Tb-doped ZnO structures for varying concentrations.

Sample	Wavenumber (cm^{-1})	Functional group
undoped ZnO	3300	O-H
	1025, 1087	C-O-C
	475	Zn-O
$Zn_{0.99}Tb_{0.01}O$	3300	O-H
	1025, 1087	C-O-C
	475	Zn-O
$Zn_{0.98}Tb_{0.02}O$	585	Zn-O
$Zn_{0.97}Tb_{0.03}O$	585	Zn-O
$Zn_{0.96}Tb_{0.04}O$	585	Zn-O
$Zn_{0.95}Tb_{0.05}O$	585	Zn-O

3.3 Optical properties

3.3.1 UV–VIS diffuse reflectance spectra

In the range of 300–700 nm wavelengths, the reflectance spectra of all $Zn_{1-x}Tb_xO$ powder concentrations gained by UV–VIS diffuse reflectance measurements (DRS) were presented in Fig. 9. Maximum reflectance was observed for $Zn_{0.97}Tb_{0.03}O$ nanorods and moreover, we observed around 96 % reflectance intensities of all compositions. The position of the wavelength is observed randomly to shift with the increasing Tb-doped concentration in ZnO as shown in Fig. 9.

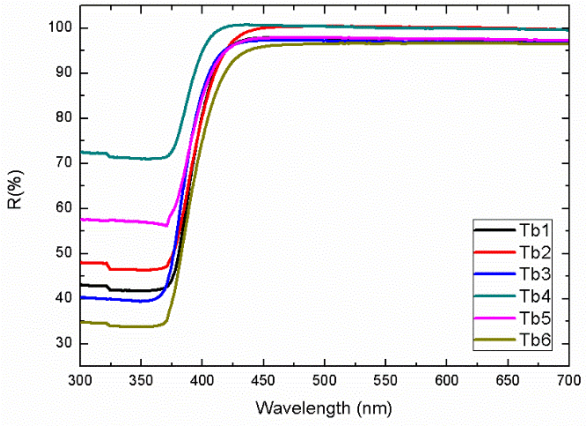

Fig. 9 The reflectance spectra of the $Zn_{1-x}Tb_xO$ powders synthesized by hydrothermal method.

3.3.2 Band Gap Calculation

The optical band gap Eg was calculated using the following equation between the photon energy (hν) and the absorption coefficient (α):

$$\alpha h\upsilon = \mathrm{k}(\mathrm{h}\upsilon - E_g)^{1/n} \quad (1)$$

In Eq. (1), k and E_g are the energy-independent constants and optical band gap, respectively. Since $F(R_\alpha)$ is proportional to α and ZnO has direct allowed transitions, n is taken as 1/2. Thus, Eq. (1) can be transformed to:

$$F(R_\alpha)\, h\upsilon = \mathrm{k}(\mathrm{h}\upsilon - E_g)^{1/2} \quad (2)$$

Also, Eq 2. could be written $(F(R_\alpha)\, h\upsilon)^2 = k^2(\mathrm{h}\upsilon - E_g)$. The band gap energies E_g are calculated by the slope of the graph of $(F(R_\alpha)\, h\upsilon)^2$ to the photon energy axis where $F(R_\alpha) = 0$, $(E_g = h\upsilon)$, as plotted in Figs. 10a-e. That is, the intersection between the linear fit and the photon energy axis gives the value of E_g. The calculated E_g values of $Zn_{1-x}Tb_xO$ samples for the compositions (x=0.0, 0.01, 0.02, 0.03, 0.04, and 0.05) were 3.2, 3.21, 3.24, 3.22 and 3.23 eV respectively. These changes in the values of the band gap energies of Tb-doped ZnO nanorods might be due to several factors such as crystallite size, carrier concentration, lattice strain, the size effect of the dopant metals in ZnO lattice.

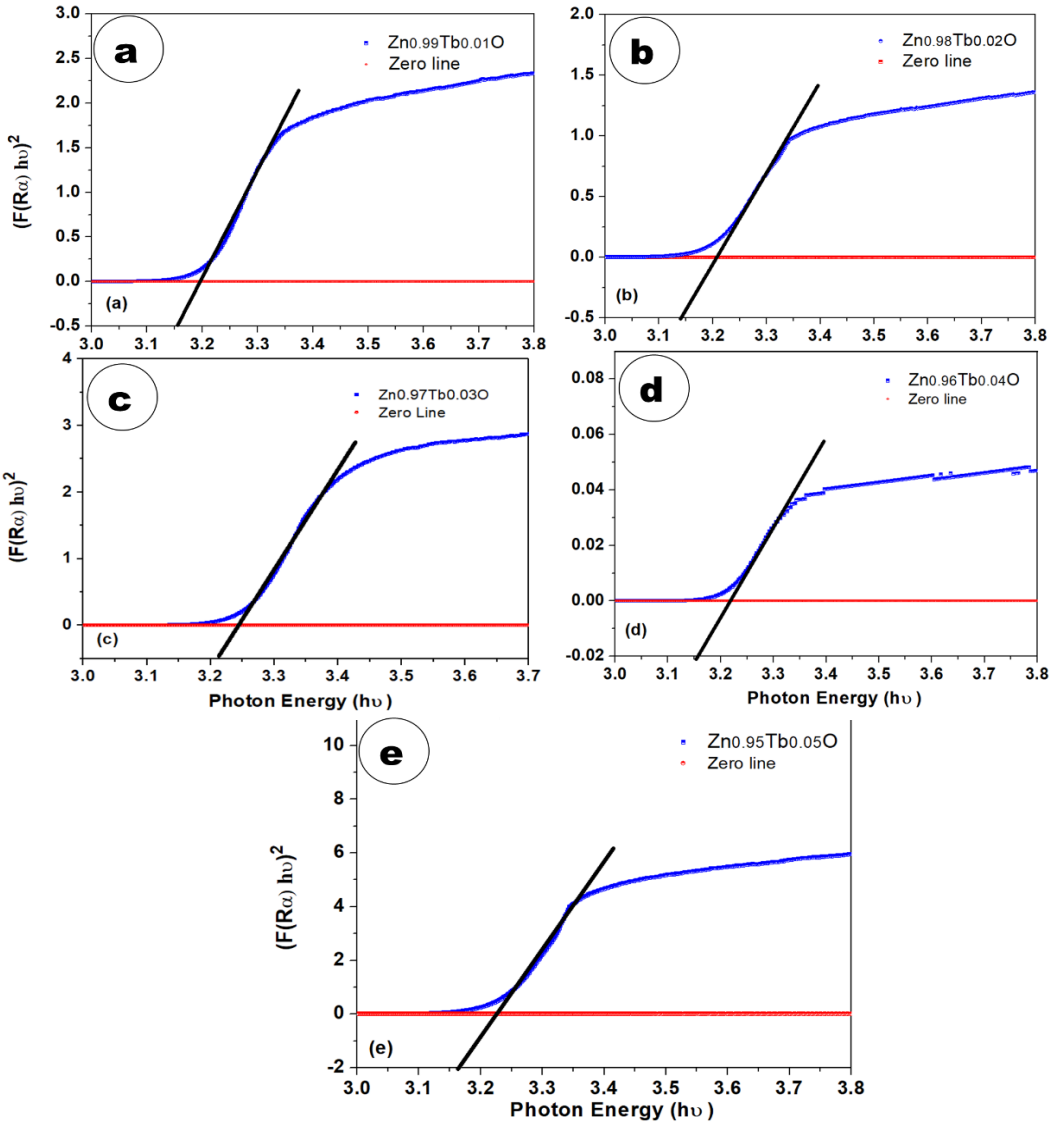

Fig. 10 The plots of $(F(R\alpha)h\nu)^2$ as a function of photon energy (hν) and the linear fit for a) x=0.01, b) x=0.02, c) x=0.03, d) x=0.04, and e) x=0.05 concentration

IV. CONCLUSION

Terbium-doped ZnO was prepared by the hydrothermal method. Its structural, microstructural, and optical properties are analyzed based on their concentration dependence. X-ray diffraction and Rietveld refinement analysis exhibited a single phase of pure and Tb-doped ZnO nanorods. The SEM picture of all ZnO and Zn1-xTbxO nanorods showed that the nanorods consisted of the almost perfect hexagonal cross-section. The larger and smaller roads showed quite different in terms of sizes from each other as well. When compared to the groups of the specimens in the SEM frame, at least five times larger in size was observed due to the increasing amount of Tb in the structures. The reflectance spectra of $Zn_{1-x}Tb_xO$ (x=0.00, 0.01, 0.02, 0.03, 0.04, and 0.05) nanorods showed that the maximum reflectance was observed for $Zn_{0.97}Tb0_{0.03}O$ concentration and the reflectance intensities of the samples were around 96 %. The band gap energies of Tb-doped ZnO nanorods were observed in the range of 3.2 - 3.24 eV. As a result the $Zn_{1-x}Tb_xO$ (x=0.00, 0.01, 0.02, 0.03, 0.04, and 0.05) nanorods with the wide band gap (E_g > 3) could be a suitable material for optoelectronics and sensor applications. The lattice parameters also exhibited almost the same fluctuation behavior with band gap energies related to the concentration rates.

REFERENCES

[1] Boyraz, C., Doğan, N. Arda, L. (2017). Microstructure and magnetic behavior of (Mg/Ni) co-doped ZnO nanoparticles. *Ceramics International*. 43, 15986-15991.

[2] S. Kaya, D. Akcan, O. Ozturk, Arda, L. (2018). Enhanced mechanical properties of yttrium doped ZnO nanoparticles as determined by instrumented

indentation technique, *Ceramics International*. 44(9) 10306-10314.

[3] Akcan, D. Gungor, A. Arda, L. (2018). Structural and optical properties of Na-doped ZnO films. *Journal of Molecular Structure*. 1161 299-305.

[4] Arda, L. Dogan, N. Boyraz, C. (2018). Effects of Annealing Temperature on Microstructure and Magnetic Properties of $Ni_{0.05}Zn_{0.95}Fe_2O_4$ Nanoparticles. *J. Supercond. Nov. Mag.* 31(2), 365-371.

[5] Boyraz, C. Yesilbas, B. Arda, L. (2017). The temperature effect on structural and magnetic properties of $Zn_{0.95}Fe_{0.05}O$ nanoparticles. *Journ. of Supercon. Nov. Mag*. 30(6), 1691–1698.

[6] Guler, A. Arda, L. Dogan, N. Boyraz, C. Ozugurlu, E. (2019). The annealing effect on microstructure and ESR properties of (Cu/Ni) co-doped ZnO nanoparticles. *Ceramics International*. 45(2), 1737-1745.

[7] Senol, S. D. Guler, A. Boyraz, C. Arda, L. (2019). Preparation Structure and Magnetic Properties of Mn-Doped ZnO Nanoparticles Prepared by Hydrothermal Method. *Journal of Superconductivity and Novel Magnetism*. DOI: 10.1007/s10948-019-5030-7.

[8] Senol, S. D. Boyraz, C. Ozugurlu, E. Gungor, A. Arda, L. (2019). Band Gap Engineering of Mg Doped ZnO Nanorods Prepared by a Hydrothermal Method. *Crystal Research and Technology*. 54 (3), 1800233.

[9] Rodnyi, P. A. and Khodyuk, I. V. (2011). Optical and Luminescence Properties of Zinc Oxide. *Optics and Spectroscopy*. 111, 776 - 785.

[10] Hassan, A. Jin, Y. Irfan, M. Jiang, Y. (2018). Acceptor-modulated optical enhancements and band-gap narrowing in ZnO thin films. *AIP Advances*. 8, 035212.

[11] Xiang, H. J. Yang, J. Hou, J. G. and Zhu, Q. (2006). Piezoelectricity in ZnO nanowires: A first-principles study. *Applied Physics Letters*. 89, 223111.

[12] Nickel, N. H. and Terukov, E. (2005). Zinc Oxide—A Material For Micro- and OptoelectronicApplications. (Springer, Dordrecht).

[13] Jeong, M. C. Oh, B. Y. Lee, W. and Myoung, J. M. (2005). Optoelectronic properties of three-dimensional ZnO hybrid structure. *Applied Physics Letters*. 86, 103105.

[14] Lu, H. Zhou, P. Liu, H. Zhang, L. Yu, Y. Li, Y. and Wang, Z. (2016). Effects of nitrogen and oxygen partial pressure on the structural and optical properties of ZnO: N thin films prepared by magnetron sputtering. *Materials Letters*. 165, 123–126.

[15] Ellmer, E. K. Klein, A. and Rech, B. (2008). Transparent Conductive Zinc Oxide, (Springer, Berlin).

[16] Reynolds, D. C. Look, D. C. and Jogai, B. (2001). Fine Structure on the Green Band in ZnO. *J. Appl. Phys*. 89, 6189.

[17] Chen, H. Gu, S. L. Tang, K. Zhu, S. M. Zhu, Z. B. Ye, J. D. Zhang, R. and Zheng, Y. D. (2011). Origins of green band emission in high-temperature annealed N-doped ZnO. *J. Lumin*. 131, 1189–1192.

[18] Yun, I. (2012). Photodiodes: From Fundamentals to Applications (InTech).

[19] Yim, K. Lee, J. Lee, D. Lee, M. Cho, E. Lee, H. S. Nahm, H. and Han, S. (2017). Property Database for Single-Element Doping in ZnO Obtained by Automated First-Principles Calculations. *Scientific Reports*. 7 40907.

[20] Blasse, G. (1979). Handbook on the physics and chemistry of the rare earth, North-Holland, Amsterdam. 4.

[21] Nazarov, M. I. Noh, D. Y. (2010). Rare earth double activated phosphors for different applications. *J. Rare Earths*. 28, 1-11.

[22] Gogotsi, Y. (2006). Nanomaterials handbook. Routledge Publishers, USA.

[23] Arda, L. (2019). The effects of Tb doped ZnO nanorod: An EPR study. *Jour. of Mag. and Mag. Mat*. 475, 493-501.

[24] Maensiri, S. Laokul, P. Promarak, V. (2006). Synthesis and optical properties of nanocrystalline ZnO powders by a simple method using zinc acetate dihydrate and poly(vinyl pyrrolidone). *Journal of Crystal Growth*. 289 102-106.

[25] Senthilkumaar, S. Rajendran, K. Banerjee, S. Chini, T. Sengodan, K. V. (2008). Influence of Mn doping on the microstructure and optical property of ZnO. *Materials Science in Semiconductor Processing*. 11, 6-12.

[26] Anna, K. Nina, P. Yuri, K. Meinhard, M. Werner, Z. Aharon, G. (2008). Coating zinc oxide submicron crystals on poly (methyl methacrylate) chips and spheres via ultrasound irradiation. *Ultrasonics Sonochemistry*. 15 839–845.

[27] Li, H. Wang, J. Liu, H. Yang, C. Xu, H. Li, X. Cui, H. (2004). Sol-Gel preparation of transparent zinc oxide films with highly preferential crystal orientation. *Vacuum*. 77 57–62.

[28] Wahab, R. Ansari, S. G. Kim, Y. S. Seo, H. K. Shin, H. S. (2007). Room temperature synthesis of needle-shaped ZnO nanorods via sonochemical method. *Appl. Surf. Sci*. 253, 7622–7626.

[29] Partha, P. Pal, J. M. (2013). Photoluminescence and thermoluminescence studies of Tb^{3+} doped ZnO nanorods. *Materials Science and Engineering B*. 178, 400–408.